The Smallest Infectious Substructure Encoding the Prion Strain Structural Determinant Revealed by Spontaneous Dissociation of Misfolded Prion Protein Assemblies

Jan Bohl, Mohammed Moudjou, Laëtitia Herzog, Fabienne Reine, Fiona Sailer, Hannah Klute, Frédéric Halgand, Guillaume van Der Rest, Yves Boulard, Vincent Béringue, et al.

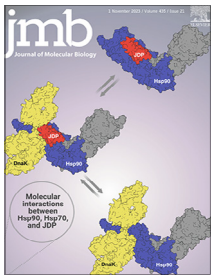

The Smallest Infectious Substructure Encoding the Prion Strain Structural Determinant Revealed by Spontaneous Dissociation of Misfolded Prion Protein Assemblies

Jan Bohl [1,2], Mohammed Moudjou [1], Laetitia Herzog [1], Fabienne Reine [1], Fiona Sailer [1], Hannah Klute [1], Frederic Halgand [2], Guillaume Van der Rest [2], Yves Boulard [3], Vincent Béringue [1,*], Angelique Igel [1,*] and Human Rezaei [1,*]

*1 - **Université Paris-Saclay,** INRAe, UVSQ, VIM, 78350 Jouy-en-Josas, France*
*2 - **ICP,** CNRS, Université Paris-Saclay, 91400 Orsay, France*
*3 - **Université Paris-Saclay,** CEA, CNRS, Institute for Integrative Biology of the Cell (I2BC), Gif-sur-Yvette, France*

Correspondence to Vincent Béringue, Angelique Igel and Human Rezaei: MAP2, VIM, INRAe, Domaine de Vilvert, 78352, Jouy-en-Josas, France. *vincent.beringue@inrae.fr (V. Béringue), angelique.igel@inrae.fr (A. Igel), human.rezaei@inrae.fr (H. Rezaei)*
https://doi.org/10.1016/j.jmb.2023.168280
Edited by Louise C. Serpell

Abstract

It is commonly accepted that the prion replicative propensity and strain structural determinant (SSD) are encoded in the fold of PrP^{Sc} amyloid fibril assemblies. By exploring the quaternary structure dynamicity of several prion strains, we revealed that all mammalian prion assemblies exhibit the generic property of spontaneously generating two sets of discreet infectious tetrameric and dimeric species differing significantly by their specific infectivity. By using perturbation approaches such as dilution and ionic strength variation, we demonstrated that these two oligomeric species were highly dynamic and evolved differently in the presence of chaotropic agents. In general, our observations of seven different prion strains from three distinct species highlight the high dynamicity of PrP^{Sc} assemblies as a common and intrinsic property of mammalian prions. The existence of such small infectious PrP^{Sc} species harboring the SSD indicates that the prion infectivity and the SSD are not restricted only to the amyloid fold but can also be encoded in other alternative quaternary structures. Such diversity in the quaternary structure of prion assemblies tends to indicate that the structure of PrP^{Sc} can be divided into two independent folding domains: a domain encoding the strain structural determinant and a second domain whose fold determines the type of quaternary structure that could adopt PrP^{Sc} assemblies.

Introduction

The prion paradigm unifies the transmission of several age-related, incurable neurodegenerative disorders based on assisted catalytical protein refolding concerted with the acquisition of quaternary structures.[1] In principle, the prion paradigm consists of an autocatalytic structural switch of a host-encoded monomeric protein or peptide induced by the same protein or peptide in an aggregated conformation.[2–5] This aggregated conformer or assembly plays the role of a template. During this assisted structural switch, the biological information encoded in the structure of the assemblies is transferred to the monomeric protein (templating step), leading to the perpetuation of the biological information.[6] In human and animal transmissible spongiform encephalopathies or prion diseases, the host-encoded cellular prion protein (PrP^{C}) undergoes an induced structural rearrangement into a

catalytical active, pathological conformation called PrP^{Sc}, which serves as a template for de novo conversion of PrP^{C} into PrP^{Sc} in an autocatalytic process.[7,8]

For conventional infectious diseases where variations in the clinical manifestation of the disease define the pathogenic strain, in prion diseases, variations in the incubation period, neuropathological patterns and biochemical properties of PrP^{Sc} assemblies differentiate prion strains.[9,10] At the molecular level, these biological differences are the consequence of differences in the structure of PrP^{Sc}. How during the replication, the strain structural determinant (SSD) is encoded in the fold of different types of quaternary structure of PrP^{Sc} assemblies in a stable manner remains unclear. Recent structural studies put in evidence structural differences at the protomer scale of brain extractive PrP^{Sc} amyloid fibrils from four different prion strains.[11–15] The SSD governs the biochemical properties of PrP^{Sc} assemblies, such as the type of PrP^{Sc} fragments generated after proteolysis,[2,16] apparent resistance to unfolding,[17,18] and size distribution of PrP^{Sc} assemblies at the terminal stage of the disease.[19–21]

In the prion literature, there is compelling evidence that different strains can be propagated on one given primary structure,[22–24] independently of the contribution of posttranslational modifications in the SSD.[11,25,26] This indicates that multiple SSDs can be encoded in one PrP primary structure. Based on our own experimental transmission data, more than fifteen different prion strains can be stably and distinctively propagated on the sheep PrP sequence ($V_{136}R_{154}Q_{171}$ allele) (Figure 1 and SI.1), indicating that one given primary PrP structure can adopt at least fifteen stable and different conformations. How such a broad diversity is structurally encoded at the scale of PrP^{Sc} assemblies remains undetermined and conceptually difficult to reconcile with the current models of prion assemblies. This question is particularly interesting when considering the large number of mammalian prion strains. At which scale – i.e., primary, secondary, tertiary, quaternary or supraquaternary PrP^{Sc} assembly structures, such a broad spectrum of structural information can be encoded remains elusive.

Putting aside the strain dimension, multiple PrP^{Sc} conformations coexist within a given prion strain.[27–29] Even if the extent of this diversity is not yet well established, it refers to the quasispecies concept, which has been proposed to be at the base of prion adaptation and strain evolution.[27] The existence of multiple conformers within a strain and, more specifically, biologically cloned strain adds another level of structural complexity to PrP^{Sc} assemblies and questions whether intrastrain structural diversity involves the SSD or another PrP^{Sc} structural subdomain. Recent investigations demonstrated

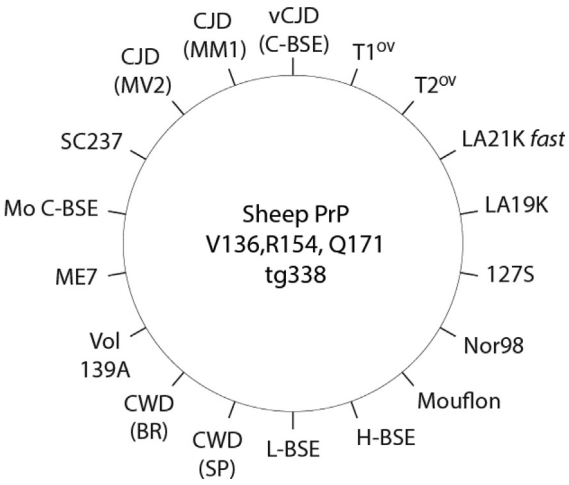

Figure 1. Different prion strains stabilized on tg338 mice expressing the allelic variant V_{136}, R_{154}, Q_{171} of sheep PrP^{C}. As shown, sheep PrP^{C} can be refolded by serving as a substrate for more than 15 different prion strains. Each fold is at the origin of a given strain structural determinant (SSD) and at the origin of the strain-specific incubation time (see SI1). The fact that a given primary structure of PrP^{C} (here sheep V_{136},R_{154}, Q_{171} variant) is able to be refolded in different structures highlights the multistability of PrP.

that, independent of the prion strain, deterministic structural diversification occurred during the replication process, leading to the formation of two sets of protease-resistant prion assemblies called PrP^{ScA} and PrP^{ScB}.[30] While for a given prion strain, PrP^{ScA} and PrP^{ScB} assemblies based on their specific infectivity are structurally different, they converge to the same strain. This suggests that different sets of assemblies from a given prion strain share the same SSD.

To determine at which PrP^{Sc} assembly structural scale the SSD is encoded and the potential variations among strains, we established a native method to disassemble PrP^{Sc} from seven different cloned prion strains into their smallest unit. We showed that, as a generic process, PrP^{Sc} from the seven prion strains disassembled into two small oligomer species, called P1 and P2. Using different size estimation methods, we determined the sizes of P1 and P2 to be tetramers and dimers, respectively. The comparison between the specific infectivity of P1 and P2 for three different strains revealed significant differences, suggesting the existence of at least two intrastrain structural subpopulations. The existence of two intrastrain subpopulations has been further confirmed by using chaotropic treatment, leading to the segregation of the initial PrP^{Sc} population into high molecular weight assemblies devoid of infectivity and an infectious small oligomeric assembly.

Results

Disaggregation of PrP^{Sc} assemblies into infectious small oligomeric assemblies

To determine how prion strain information is encoded in the PrP^{Sc} structure, we established native disassembling conditions to disaggregate PrP^{Sc} assemblies into their elementary subunit suPrP. Brain homogenates (BHs) of seven different prion strains from hamster and transgenic mice expressing ovine (tg338) and mouse (tga20) PrP were proteinase K (PK)-digested to remove PrP^{C} before a 4-hour solubilization step at 37 °C in a buffer containing dodecyl maltoside and sarkosyl at 5 mM and 50 mM, respectively (see M&M for more details). At these concentrations, these two detergents do not significantly affect either protein tertiary structure[31,32] or prion infectivity.[19,21,30] The solubilization procedure led to a translucid solution. After a subsequent centrifugation step at 15,000*g,* the supernatants and the pellets were collected and analyzed for PK-resistant PrP^{Sc} (PrP^{res}) content by western blotting. The pellets contained negligible amounts of PrP^{res} compared to the supernatants (see SI2). The supernatants were then directly analyzed by size exclusion chromatography (SEC) using a running buffer that did not contain any detergent to avoid the formation or maintenance of lipidic micellar structures that could interfere with the intrinsic elution volume of PrP assemblies.[32,33] The collected fractions were analyzed by western blotting for PrP^{res} content. As typically shown for cloned ovine LA21K *fast*, LA19K, and hamster 263 K prion strains, the chromatograms revealed the existence of two discreate and well-defined PrP^{res} peaks called P1 and P2, indicating the presence of at least two sets of oligomeric PrP^{res} assemblies (Figure 2(-A-C)). For LA21K *fast*, LA19K and 263 K, the SEC analyses of mouse ME7, 139A, 22L, and Fukuoka-1 prion strains revealed similar elution profiles. Only the relative proportions of P1 and P2 varied among the strains analyzed. The seven strains tested here thus share a common disassembly process generating P1 and P2 (Figure 2(D)). According to our calibration, the hydrodynamic radius of the assemblies in P1 and P2 ranged between a trimer and tetramer of PrP for P1 and a PrP dimer for P2. Each injection was repeated at least three times, with only minor deviations in the elution profiles (see error bars in Figure 2), demonstrating the high repeatability of the SEC experiments.

To determine whether purified infectious fibrillar PrP^{Sc} follows a disassembly pathway similar to that of PrP^{Sc} present in the brain homogenate, we first purified PK-treated 263 K assemblies according to Wenborn and colleagues' protocol.[34] The hydrodynamic radius as well as the mean average molecular weight (<Mw>) of these purified assemblies as estimated by static (SLS) and dynamic light scattering (DLS) revealed a <Mw> of 8 MDa with a hydrodynamic mean average radius of the assemblies centered at approximately 150 nm (Figure 3(A)). The purified 263 K at 20 nM (concentration expressed equivalent to monomer) was then incubated at 37 °C under identical conditions as for BH (Figure 2(C)) before analysis by SEC coupled to SLS. As shown in Figure 3(A and B), when initially the size of purified 263 K was approximately 150 nm with a <Mw> of approximately 8 MDa, after solubilization, SEC revealed a single unique peak eluting at the P2 position, with a mean average molecular weight of $\approx 54kDa$ (Figure 3(B)), which is in good agreement with a dimeric N-terminal truncated mixture of mono- and biglycosylated PrP. This observation indicates that after solubilization, the very large assemblies initially present in the purified products were transformed into P2 species. However, when PrP^{Sc} present in the brain homogenate gave rise to two peaks, P1 and P2, the disassembly of purified 263 K gave a unique peak eluting at the P2 position.

To precisely determine the molecular weight of PrP^{res} assemblies present within the P1 and P2 peaks, a crosslinking approach was adopted using BS3 as an 11 Å bifunctional amine crosslinker to covalently trap the oligomeric state. After SEC, collected fractions corresponding to P1 and P2 from 263 K and LA21K *fast* were incubated with 0.5 or 2 mM BS3 to covalently crosslink lysine residues distant below 11 Å (see materials and methods). The analysis of crosslinked P1 and P2 by western blot revealed the existence of dimeric bands (Figure 3(C and D)) for both strains. Other minor PrP multimeric bands, such as trimer and tetramer bands, were also observed. However, their ratio did not evolve with higher amounts of BS3, indicating that the dimeric species in the P1 and P2 peaks are preferentially crosslinked by BS3.

Thus, according to the hydrodynamic radius estimation, the mean average molecular weight determination by SLS and the crosslinking experiments, the quaternary structure of P2 species corresponds to a dimer. According to their hydrodynamic radius, the size of objects forming the P1 peak are expected to range between a trimer and a tetramer of PrP. However, the crosslinking experiment tends to indicate a dimer. This discrepancy can be explained if P1 corresponds to a dimer of dimer, the crosslinking events being more favorable in the dimer due to the proximity of BS3 reacting groups.

The dynamics of P1 and P2 oligomers

To determine if P1 is a condensate of P2 assemblies, dilution experiments were performed prior to solubilization and SEC analysis. As typically shown for the 263 K, LA21K *fast* and LA19K strains, P1 oligomers progressively disassembled into smaller oligomers eluting at the elution volume corresponding to the P2 peak position (Figure 4(A-C)). For these three strains,

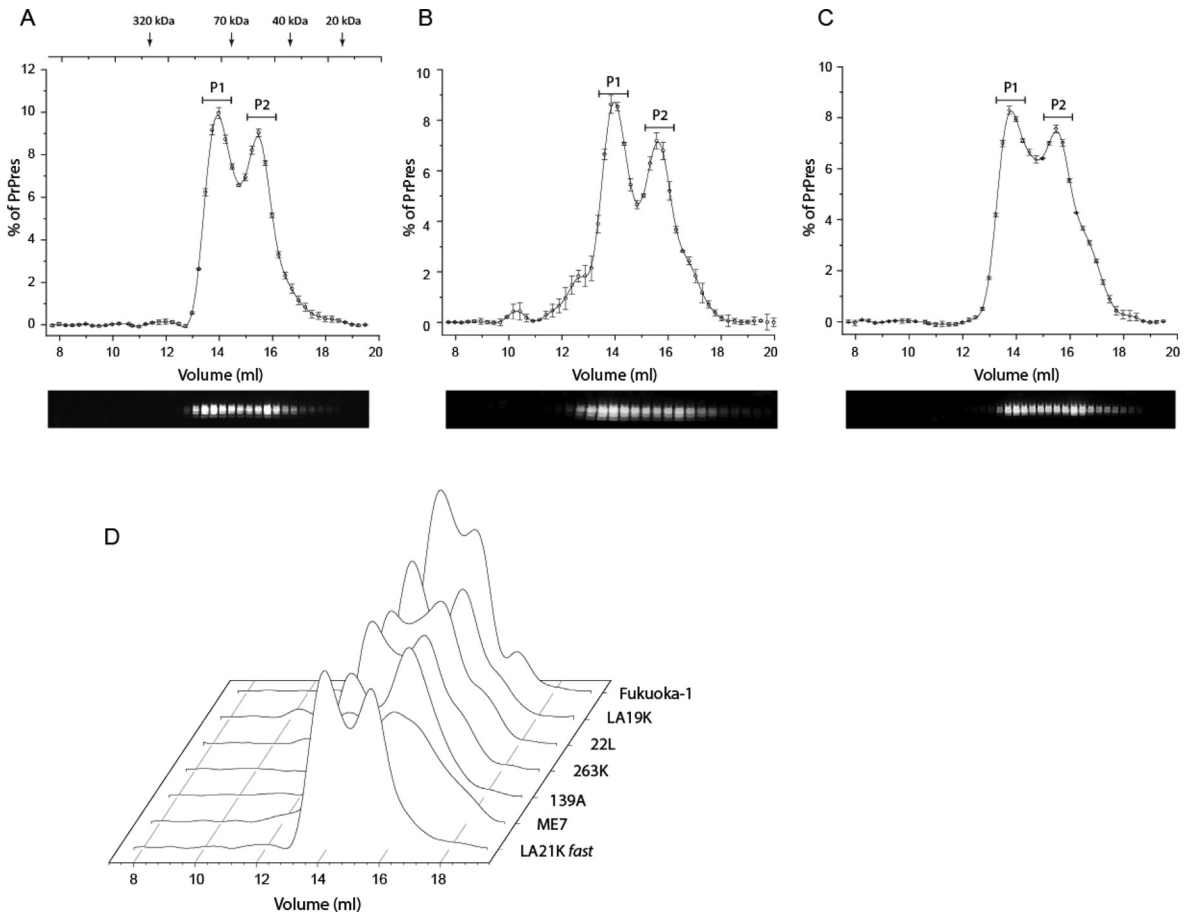

Figure 2. Analysis of the quaternary structure of PrP^{res} assemblies by SEC. Chromatograms of solubilized PK-treated brain homogenates containing LA21K *fast* (A), LA19K (B) and 263 K (C) prions. The mean levels of PrP^{res} per fraction were obtained from the immunoblot analysis of $n = 3$ independent SEC. Representative western blots used for PrP^{res} level quantification are presented below the chromatograms. For the three strains, the chromatograms revealed the presence of two discreet peaks called P1 and P2. The same analysis for four other strains (ME7, 139A, 22L and Fukuoka-1, (D).

the P1 dissociation started with a dilution factor of two, and this dissociation was concerted with a progressive translation of the P1 peak toward the P2 peak (Figure 4(A-C)). Similar results were obtained with 22L, Fukuoka-1, ME7 and 139A prion strains (Figure 4(D)), indicating that oligomeric assemblies in P1 result from the polymerization of smaller oligomers eluting at the P2 peak position. The fact that P2 from the seven prion strains tested have the same elution volume or partition coefficient (K_{AV}) (Figure 4(E)) indicates an equivalence for P2 oligomer hydrodynamic size and thus consequently a comparable quaternary structure.

The depolymerization of P1 into P2 induced by dilution tends to indicate that weak interactions are involved in the cohesion of the P1 quaternary structure. To increase the strength of these interactions and to investigate the possibility of P1 and P2 condensing into larger assemblies, we explored the effect of ionic strength variations (from 200 mM to 20 mM NaCl) on the quaternary structure of P1 and P2 (Figure 4(F,G)). As shown for 263 K and LA21K *fast*, the decrease in ionic strength caused the disappearance of P2, a shift in the size of P1 and the formation of very large assemblies (size >400 kDa). These observations indicate that i) P2 oligomers can polymerize into larger assemblies, and ii) as variations in ionic strength substantially affect PrP size distribution, weak electrostatic interactions govern the condensation dynamics.

Specific infectivity and replicative propensity of P1 and P2 oligomers

To determine P1 and P2 infectivity, pools of SEC fractions corresponding to the P1 and P2 peaks from 263 K, LA21K *fast* and LA19K prions were intracerebrally inoculated into adequate reporter transgenic mice. By considering the short incubation times in reporter mice for 263 K and LA21K *fast*,[19] two dilutions were inoculated. The

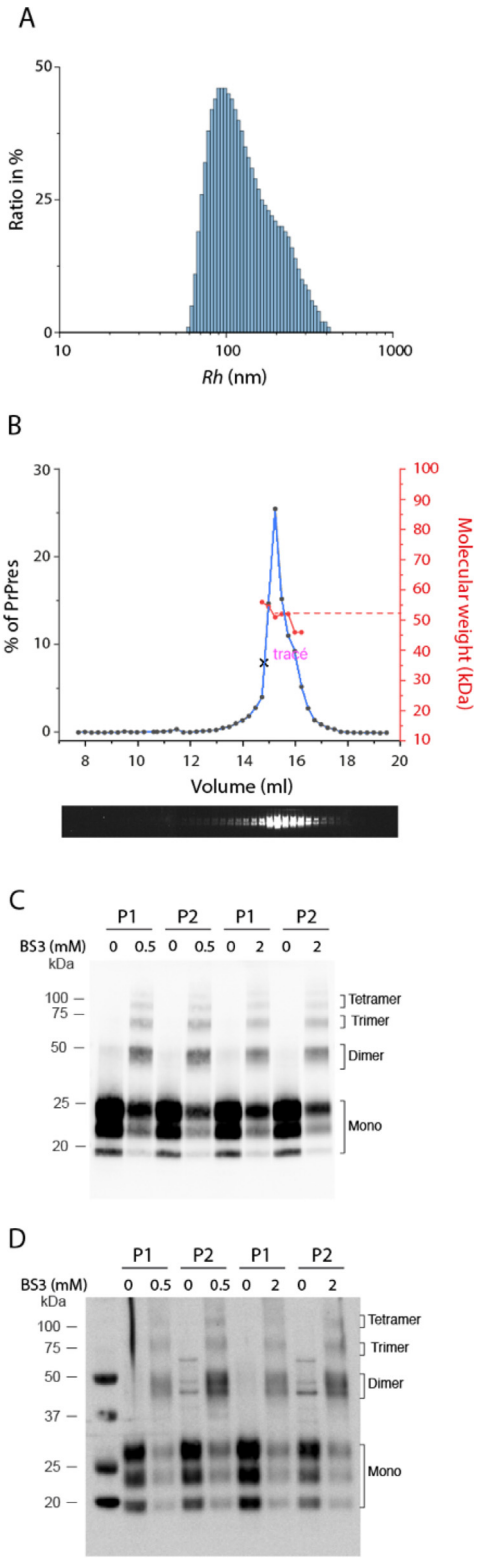

Kaplan-Meier curves describing the survival percentage as a function of time post-inoculation are depicted in Figure 5(A). P1 and P2 from the three strains induced disease at the full attack rate. However, for the three strains and the two dilutions tested for 263 K and LA21K *fast*, the P2 incubation time was significantly shorter than the P1 incubation time. We next determined the specific infectivity of the PrP^{Sc} assemblies populating P1 and P2, i.e. the amount of infectivity divided by the amount of PrP^{res} per peak. For the three strains, the estimation of P1 and P2 infectivity was based on the ad hoc dose response curves[19] and materials and methods). The amount of PrP^{res} per peak was estimated based on the percentage of PrP^{res} reported on chromatograms (see SI3). The specific infectivity of the assemblies eluting under P2 peak was 15-100-fold higher than that of the P1 peak (Figure 5 (B)). On the other hand, the strain phenotypes of P1 and P2, as assessed by their PrP^{res} electrophoretic signature (Figure 5(C)) and regional distribution of PrP^{res} in the brain (Figure 5(D)), were globally superimposable and resembled those of the parental strains.[24,35] For 127S or LA21K *fast* strains, the PrP^{res} deposition profile in the brain, specifically in the corpus callosum and subcortical regions, depends on the inoculated dose of prions.[36] As shown in Figure 5(D) (see also SI4), these regions were PrP^{res}-positive after injection of both P1 and P2 (Figure 5(D)) while inoculation of diluted P1 and P2 did not induce deposition (SI4). Therefore, it seems unlikely that lower infectivity of P1 is due to P1 and P2 peak overlapping and fractionation procedure.

Figure 3. Size characterization of P1 and P2 assemblies. (A) Hydrodynamic radius (Rh) of purified 263 K assemblies as estimated by static light scattering (SLS). (B) SEC analysis of purified 263 K assemblies solubilized under the same conditions as for brain homogenate. The light scattered intensity measurement of the fractions corresponding to the P2 peak allows us to estimate the <Mw> of assemblies eluting at the P2 position. By neglecting the edge effect, the maximum of the peak corresponds to <Mw> of 54 kDa, compatible with a PrP^{res} dimer core. (C-D) Western blot profile of SEC fractions corresponding to P1 and P2 from 263 K (C) and LA21K fast (D) PrP^{res} before and after crosslinking with different concentrations of BS3 (0.5 and 2 mM). BS3 crosslinking led to the appearance of mainly a dimeric band even at high concentrations. Independent of BS3 concentration, other minor PrP multimeric bands, such as trimer and tetramer bands, were also observed, suggesting a dynamic exchange between higher quaternary structure arrangements.[54]

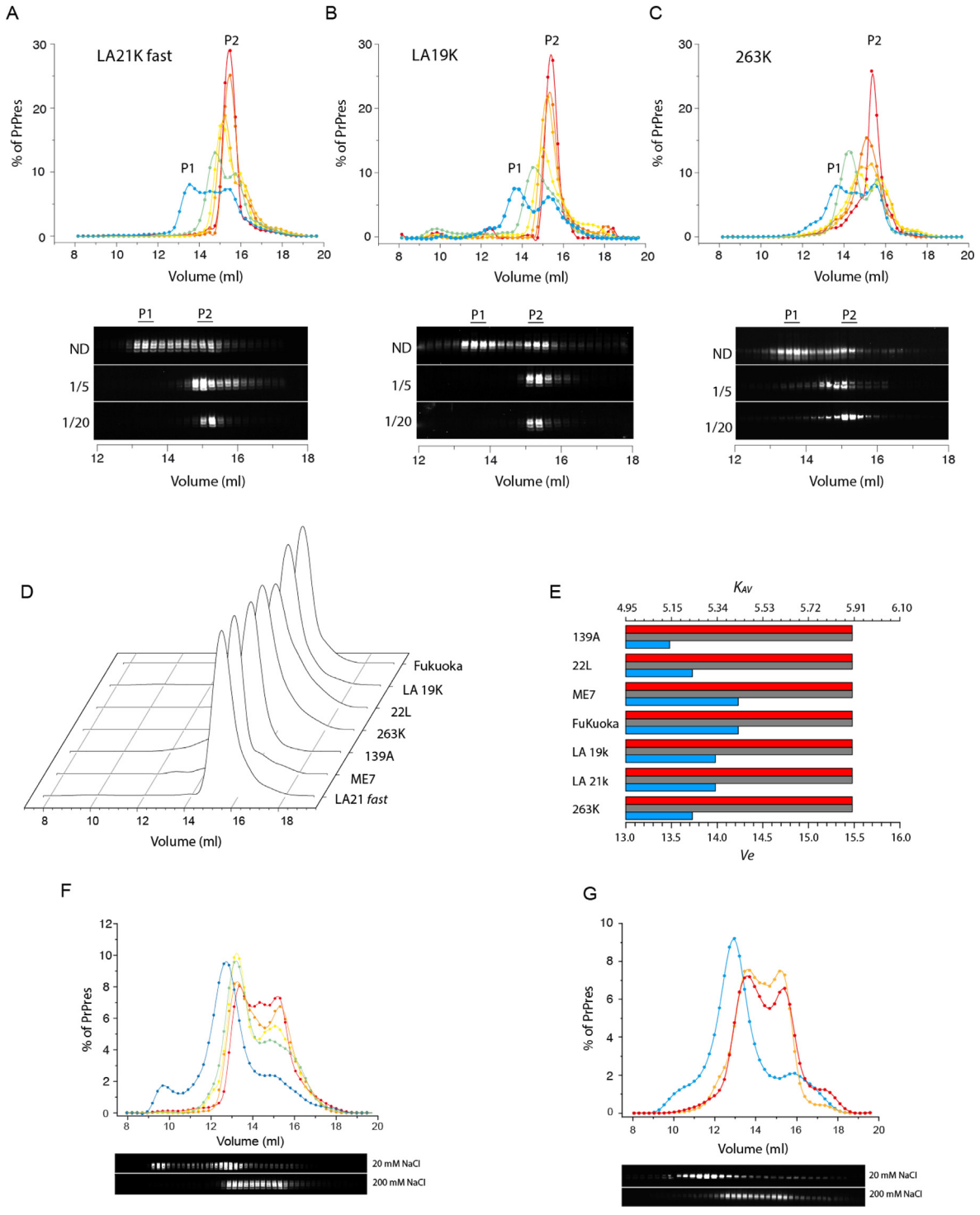

Figure 4. Effect of dilutions on the quaternary structure of P1 and P2 assemblies. (A-C) SEC chromatograms showing the effect of dilution on the size distribution of PrP^{res} assemblies from LA21K *fast*, LA19K and 263 K strains. From blue to red, the dilution factors are 1, 2, 3, 5, 10 and 20. Representative western blots used for PrP^{res} level quantification are presented below the chromatograms. (D) Chromatograms representing the effect of a 10-fold dilution factor for seven different prion strains. (E) Representation of chromatogram peak positions reported as the volume of elution (*Ve*) or average distribution constant (K_{AV}) for the seven prion strains. The gray and blue bar graphs represent the P2 and P1 peak positions before dilution, respectively (Figure 2(A-C)), while the red bar graphs represent the peak positions after 10-fold dilution. (F-G) Dependency of the quaternary structure of PrP^{res} assemblies from LA21K *fast* (F) and 263 K (G) on the ionic strength of the solubilization media. The blue curve corresponds to ionic strength relative to 20 mM NaCl, and the red curve corresponds to 200 mM NaCl. Representative western blots used for PrP^{res} level quantification are presented below the chromatograms.

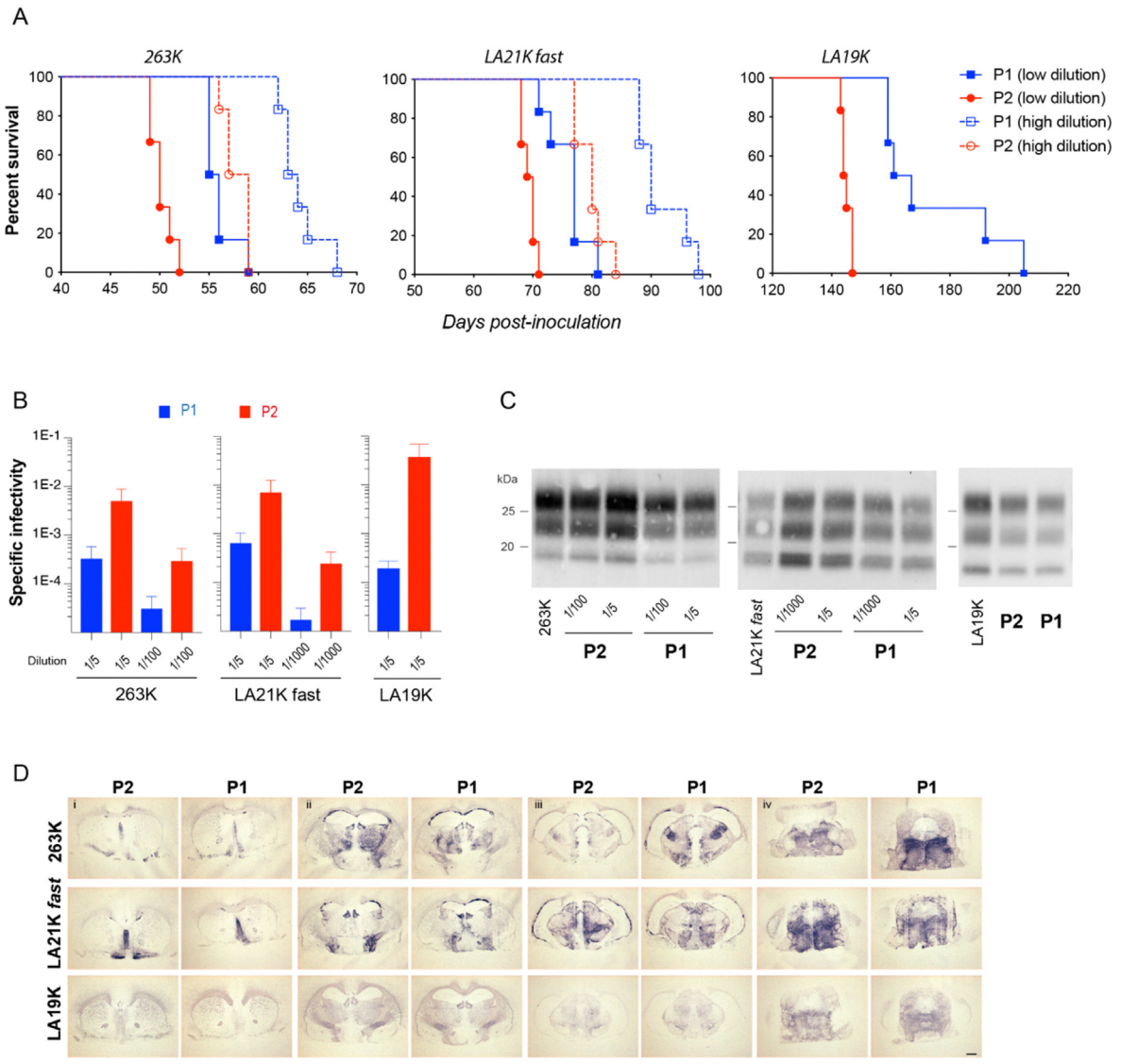

Figure 5. Biological activity of the P1 and P2 assemblies. P1 and P2 assemblies from 263 K, LA21K *fast* and LA19K prions were intracerebrally inoculated into reporter tg7 mice expressing hamster PrP (263 K) and tg338 mice expressing ovine PrP (LA21K *fast*, LA19K). (A) Kaplan-Meier curves plot the percentage of mice without prion disease (survival) against the incubation time (days postinoculation). The blue and red colors correspond to the inoculation of P1 and P2, respectively. For 263 K and LA21K *fast,* P1 and P2 were inoculated at low and high dilutions (plain lines correspond to 1:5 dilution for all three strains; dashed lines correspond to 1:100 dilution for 263 K or 1:1000 dilution for LA21K *fast*). The difference between the P1 and P2 survival curves was statistically significant according to the Mantel-Cox test at all dilutions tested. (B) Specific infectivity of the P1 and P2 peaks post-SEC fractionation (amount of infectivity divided by the amount of PrP^{res}), as calculated from the mean survival time of mice using dose–response curves (infectivity) and the percentage of PrP^{res} reported on chromatograms (amount of PrP^{res} per peak). The differences in the specific infectivity values were statistically significant ($p < 0.05$, Mann-Whitney test). (C) Electrophoretic pattern of PrP^{res} in the brains of mice inoculated with P1 and P2 assemblies. The pattern found after inoculation of unfractionated material is shown for comparison. (D) Representative histoblots of rostro-caudal transversal brain sections after challenge with P1 and P2 assemblies from 263 K, LA21K *fast* (1/5 dilutions) and LA19K prions. Analyses were performed at the level of the septum (i), hippocampus (ii), midbrain (iii) and brainstem (iv). Histoblots were probed with 3F4 (263 K) and 12F10 (LA21K *fast*, LA19K) anti-PrP monoclonal antibodies, as indicated. Scale bar, 1 mm (for higher dilution see SI4).

The difference in specific infectivity indicates that the structural properties of the assemblies present in the P1 peak are different from those present in P2 to confer distinct replicative properties. The structural difference between P1 and P2 also indicates that P1 does not result from a simple condensation of P2 but a transformation that requires a structural rearrangement.

Urea unfolding reveals the existence of two sets of assemblies

To further ascertain the structural differences between P1 and P2, we explored the evolution of the P1 and P2 peaks as a function of the concentration of a chaotropic agent such as urea. As shown for LA21K *fast*, LA19K, and 263 K, a global quaternary structure rearrangement was observed as a function of urea concentration (Figure 6(A-C)). Increasing urea concentration led to a progressive disappearance of P2 and P1 oligomers. Unexpectedly, this was concerted with the formation of a set of higher molecular weight assemblies called $P0^U$ with an elution volume lower than P1 and a set of assemblies called $P1^U$ with an elution volume slightly higher than P1. The four other prion strains behaved similarly to urea treatment even if the size and amount of $P0^U$ was strain-dependent, suggesting a common structural rearrangement dynamic (Figure 6(D)). The fact that during urea exposure two sets of PrP^{Sc} assemblies are spontaneously generated suggests the existence of two initial, structurally distinct sets of PrP^{Sc} assemblies responding differently to urea treatment.

Among the prion strains tested, the $P0^U$ and $P1^U$ of LA21K *fast* are the best separated by SEC and are in quasi-equal amounts at 6 M urea (Figure 7 (A)). An intermediate PrP^{res} population eluting between $P0^U$ and $P1^U$ at 11.5 ml is also observed. We thus used this strain to further evaluate the

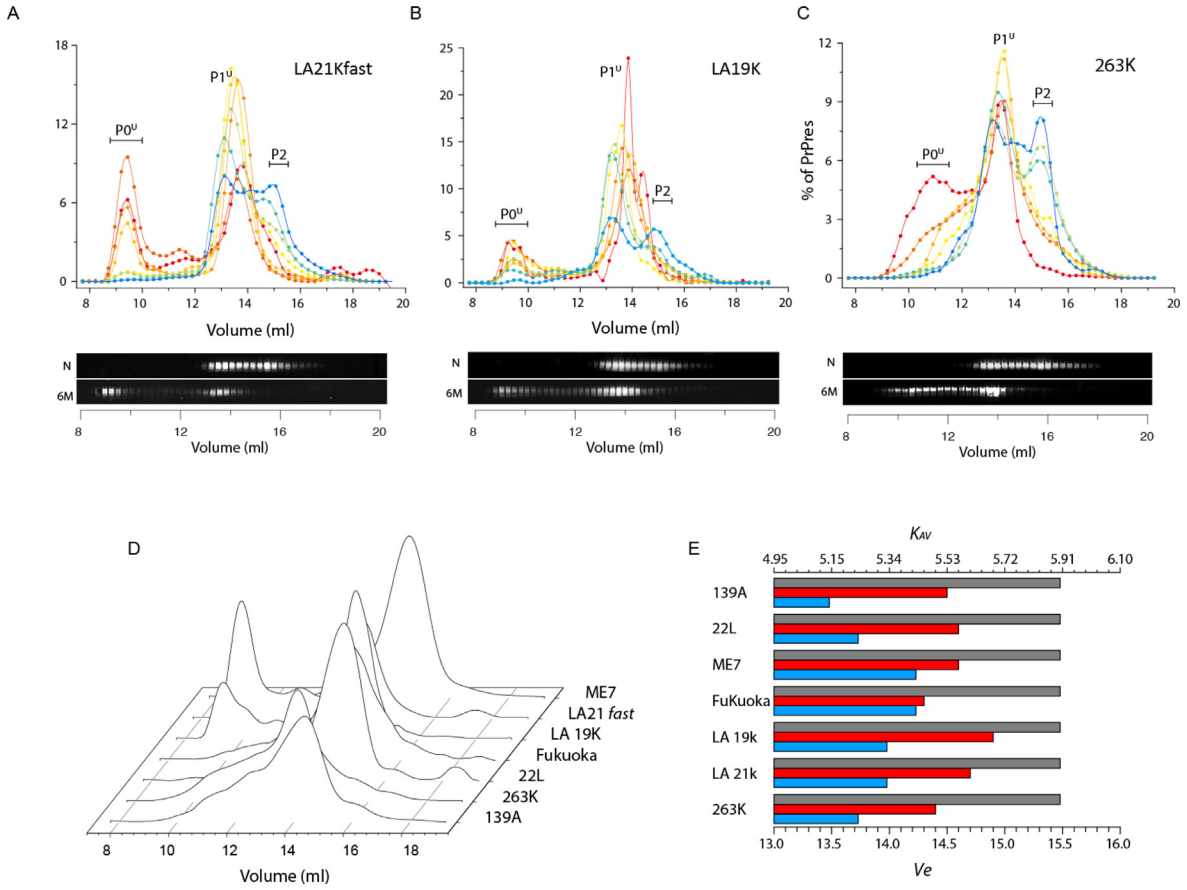

Figure 6. Effect of partial unfolding on the quaternary structure of PrP^{res} assemblies. Typical chromatograms representing the effect of increasing urea concentration on the size distribution of PrP^{res} assemblies for LA21K *fast* (A), LA19K (B) and 263 K (C) strains. For the three strains, the P2 peak progressively disappears as a function of increasing urea concentration in favor of the emergence of a new peak called $P0^U$ corresponding to very large assemblies eluting almost at the void volume of the column and $P1^U$ eluting at the same elution volume as P1. For each strain, typical western blots of SEC fractions corresponding to native conditions (N) and 6 M urea are presented. Chromatograms corresponding to the effect of 6 M urea treatment on four more strains are also presented (D). For the previous three strains, 6 M urea treatment of 139A, 22L, Fukuoka and ME7 was conducive to the formation of larger assemblies $P0^U$ and $P1^U$. (E) Representation of chromatogram peak positions reported as the volume of elution (*Ve*) or average distribution constant (K_{AV}) for the seven prion strains. The blue and red bar graphs represent the P1 and $P1^U$ peak positions, respectively (Figure 6(A-D)). For comparison, the peak position of P2 is also represented (in gray).

templating activity as well as the biochemical differences between $P0^U$ and $P1^U$. The infectivity and templating activity were estimated by bioassay in tg338 reporter mice and by PMCA using the tg338 mouse brain as a substrate (Figure 7(B and C)). As shown, $P1^U$ induced disease at a 100% attack rate, albeit with a delayed mean incubation time of 104 ± 2 days, compared to P1 and P2. Reporting this value to the LA21K *fast* dose–response curve allowed us to calculate that $P1^U$ peak infectivity was equivalent to that present in 1.4×10^5 diluted LA21K *fast* brain material. It also indicated that $P1^U$ was >200-fold and >2500-fold less infectious than P1 and P2, respectively. Mice inoculated with $P0^U$ did not develop the disease up to 250 days postinoculation (Figure 7(B)). The incubation time of LA21K *fast* at the limiting dilution dose (10^{-7}) is approximately 150 days,[24] indicating the absence of infectivity in $P0^U$ as measured by this bioassay. Further analysis of $P0^U$ templating activity by PMCA, which is a more sensitive method,[37] showed that $P0^U$ seeding activity was at least 1000-fold lower than that of $P1^U$ (Figure 7(C)). Moreover, the PMCA templating activity graph presents a plateau for an intermediate PrP population eluting at 11.5 ml between $P0^U$ and $P1^U$ (indicated by an arrow in Figure7(C)). This plateau is even more pronounced with 263 K (SI3). The formation by urea treatment of a higher order quaternary structure than $P1^U$ with significant PMCA templating activity highlights a structural rearrangement of PrP^{res}, generating *de novo* an oligomer harboring a replicative activity. The formation of such species also tends to indicate that $P1^U$ infectivity/templating activity does not correspond to remanent P1 infectivity/templating activity.

Both the bioassay and the PMCA assay indicate that $P0^U$ and $P1^U$ have different infectivity and replicative activity and thus are structurally different. These findings further suggest the existence of two structurally distinct sets of assemblies initially present within LA21K *fast* that evolved differently during urea treatment.

Discussion

The structural diversity of prion assemblies can be qualitatively considered at two scales. At the interindividual scale, it defines the prion strain or prion field isolate. The extent of this diversity at least equals the number of prion strains identified thus far.[10,38,39] At the strain scale, the structural diversity reflects the coexistence of PrP^{Sc} subpopulations (or substrain conformers).[27,30] The actual dogma considers the strain information encoded in the structure of PrP^{Sc} assemblies when intrastrain structural variations can be defined as the structural diversity of PrP^{Sc} assemblies within a strain. How and in which PrP protein domain(s) both the intra- and the inter-strain diversity could be structurally encoded in a stable manner during multiple replication events remains an open question. The propagation of almost 20 different prion strains in tg338 mice expressing sheep PrP reported as an example in Figure 1 well demonstrates the complexity of the system.

A common dimeric quaternary structure harbors the strain structural determinant

We previously reported that partial unfolding of PrP^{Sc} assemblies is conducive to the formation of a small oligomeric object called suPrP harboring

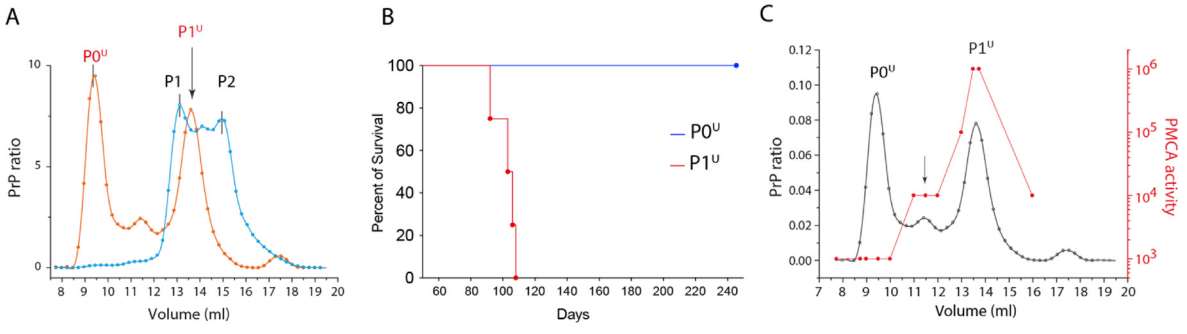

Figure 7. Specific infectivity and PMCA activity of $P0^U$ and $P1^U$ from LA21K *fast*. (A) Chromatogram showing the separation between $P0^U$ and $P1^U$ at 6 M urea (in red). Comparison chromatogram indicating the P1 and P2 positions under native conditions (in blue). (B) Survival of tg338 mice intracerebrally injected with fractions corresponding to the $P0^U$ peak (in blue) and $P1^U$ peak (in red). (C) LA21K *fast* 6 M urea chromatogram (in black) and PMCA templating activity measurement of eluted fractions (in red). The arrow indicates the position of an intermediate PrP^{res} subpopulation where the PMCA templating activity presents a step. Similar observations were made with 263 K in presence of 6 M urea (see SI3).

replicative and strain information.[40] In the present work, we show that in biochemical conditions that can be considered native in terms of infectivity and the fold of strain structural determinant,[19,21,30–32] PrP^{Sc} assemblies spontaneously dissociated into two sets of small infectious oligomeric species, which are called P1 and P2 with respect to their respective elution volumes by SEC. The determination of the molecular weight of the assemblies in the P2 peak by three distinct methods (static light scattering, covalent crosslinking, and hydrodynamic radius estimation) tend to suggest a dimeric quaternary structure. Bioassays in relevant transgenic mice demonstrated that P1 and P2 species conserve replicability and strain properties.

Currently, there is a consensus that both prion infectivity and SSD are encoded in the PrP^{Sc} amyloid fibril fold, even if other quaternary arrangements are increasingly evocated to harbor replicative propensity.[35,40,41] The fact that small dimeric species such as P1 and P2 harbor both infectivity and strain structural determinants shows that prion replicative properties are not restricted to the fibrillar fold and can also be contained in non-fibrillar arrangements of PrP. We demonstrate that the disassembly process and the dimeric structure of P2 are conserved for seven different prion strains from three distinct mammalian PrP species. Based on the diversity of the tested strains, the different host PrP sequences and the reproducibility of the results, we consider that the disassembly process and the P2 dimeric quaternary structure are generic for all mammalian prions. Such common behavior inevitably allows us to conclude that the strain information is not defined by the size of the PrP^{Sc} elementary brick as we previously hypothesized[40] but is defined by the conformation of this dimer. However, considering the growing number of prion strains (considering natural and experimental strains roughly close to 50,[10,29,38,39] it is not trivial to imagine how such diversity could be encoded in a common dimeric quaternary structure in a stable manner during multiple replication events without affecting the stability of the oligomerization interface. Such a thermodynamic paradox can be circumvented if the oligomerization domain (i.e., dimerization interface) is structurally independent from the domain encoding the strain information. According to this hypothesis, the domain harboring the SSD could be qualified as a variable domain, differing from one strain to another, while the oligomerization domain would present less variability from one strain to another. The quasi-independence of the polymerization domain from SSD also constitutes the best explanation in the limit of current strain typing methods of why different PrP^{Sc} subpopulations within a given strain, such as fibrillar and nonfibrillar PrP^{Sc},[30,41,42] harbor the same strain information despite their quaternary structure difference.

Existence of two conformationally distinct sets of assemblies

Bioassays with relevant transgenic mice and *in vitro* templating activity measurements systematically showed that the specific infectivity and the templating propensity of P1 assemblies from 263 K, LA21K *fast* and LA19K prions differ substantially from P2, even if the general strain properties are conserved. These differences are the hallmark of the existence of at least two structurally distinct PrP^{Sc} subpopulations within prion strains. Urea-induced unfolding experiments confirmed this structural polydispersity. The process of urea unfolding gives rise to the formation of two quaternary distinct sets of PrP^{Sc} assemblies. The progressive disappearance of P2, a shift in P1 toward $P1^{U}$ and the formation of large assemblies $P0^{U}$ indicate a profound rearrangement of the quaternary structure of PrP^{Sc} assemblies upon urea treatment. Even if $P1^{U}$ and $P0^{U}$ amounts and their respective K_{av} are strain specific, the seven prion strains analyzed here behave similarly during urea unfolding, suggesting that the existence of two intrastrain subpopulations is a generic property of mammalian prions.

In the case of LA21K *fast* prions, where $P1^{U}$ and $P0^{U}$ are well separated by SEC, the measures of infectivity and templating activity indicate that $P1^{U}$ is infectious, while $P0^{U}$ is not infectious and has very low PMCA-templating activity. Only the initial existence of two structurally distinct sets of assemblies could give rise to the formation of at least two quaternary distinct sets of assemblies, $P1^{U}$ and $P0^{U}$, with substantial differences in infectivity, templating activity, and quaternary structure.

To explain the specific biochemical properties of $P0^{U}$ and $P1^{U}$, the P1 and P2 structural domains involved in quaternary structure organization and SSD should have different stabilities with respect to urea denaturation (Figure 8(A)). Since the formation of $P0^{U}$ correlates with the disappearance of P2, one can hypothesize that during urea unfolding, the SSD of P2 assemblies could unfold, releasing structural constraints that will allow the modification of the quaternary structure and the formation of larger assemblies as $P0^{U}$. This specific unfolding of the SSD causes the resulting assemblies to lose their strain characteristics and infectivity. In contrast, the formation of $P1^{U}$ could result from the partial unfolding of the polymerization domain of P1 due to its lower stability. This partial unfolding is accompanied by a structural rearrangement of the PD domain of P1, leading to a more compact oligomer $P1^{U}$. This change in compactness also explains the slight shift in the elution volume (or K_{AV}) of $P1^{U}$ compared to P1, as systematically observed for all the strains tested here.

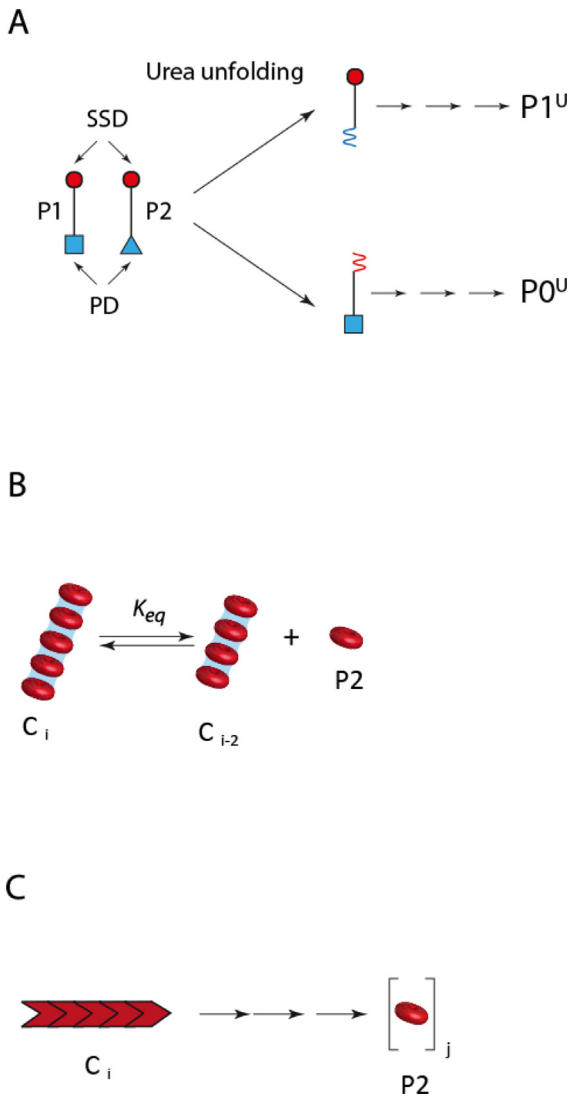

Figure 8. (A) Hypothetical mechanism of how urea unfolding induces the evolution of P1 and P2 toward $P0^U$ and $P1^U$. Urea treatment induces a different structural rearrangement in PrP^{Sc} assemblies' polymerization domain (PD), leading to the formation of two new quaternary structures $P0^U$ and $P1^U$. The formation of two distinct set of assemblies $P0^U$ and $P1^U$ with highly significant differences in there biochemical and biological properties can be explained if one considers that the SSD domain of P2 is more sensitive to urea unfolding leading to $P0^U$ while the SSD of P1 is more stable and resists to urea unfolding, leading to $P1^U$. (B-C) Two types of mechanism can explain the formation of P2 species from amyloid fibrils. (B) PrP^{Sc} fibrils and P2 could represent two different phases of the same object in equilibrium. According to this hypothesis, P2 would constitute the fibrils elementary subunit. (C) P2 would result from a structural rearrangement of the amyloid fibrils at the protomer scale.

The existence of two structurally distinct PrP^{Sc} within a given prion raises the question of how they can be generated during the process of prion replication and how they can be maintained. We previously reported that the early step of replication is associated with deterministic structural diversification, giving rise to two specific subpopulations called PrP^{Sc}A and PrP^{Sc}B.[30,35] During the evolution of the pathology, PrP^{Sc}A disappears in favor of PrP^{Sc}B according to a secondary templating pathway that requires the presence of PrP^C. Even if proof of the equivalence between these two early generated species and P1 and P2 is not established, we show here that whatever the prion strains tested, the structural diversity continues to be maintained throughout the evolution of the pathology, indicating a coevolution of two structurally distinct subpopulations. Bioassay and PMCA experiments demonstrated that P1 assemblies present lower specific infectivity and templating activity than P2 assemblies, suggesting that during multiple replication events, P2 species should be selected based on the best replicator selection principle. The only way (and nonother exist) to escape the best replicator selection principle is the existence of a pathway of spontaneous or assisted transformation of P2 to P1.

The high dynamicity of PrP^{Sc} assembly contrasts with a canonical amyloid structure

The effects of dilution and ionic strength on the quaternary structure of P0, P1 and P2 highlight the dynamicity of PrP^{Sc} assemblies. This dynamic balance between a highly aggregated state and the dimeric state fundamentally contrasts with the canonical amyloid fold of prion infectious particles. The cryo-EM structures reveal a single-strand amyloid organization with protomers in a parallel-in-register intermolecular β-sheet (PIRIBS)-based fold.[11–14] As we show here, purified 263 K PrP^{Sc} assemblies spontaneously evolve (thermodynamically speaking) from a highly aggregated state into dimeric P2 species. Even if the condition of this transformation requires the presence of detergents, such as dodecyl maltoside, sarkosyl and incubation at 37 °C, it highlights the existence of a transformation pathway between PrP^{Sc} amyloid fibrils and the dimeric P2 species that does not significantly affect the original SSD but deeply affects the quaternary structure organization.

Two hypotheses can explain the relationship between PrP^{Sc} amyloid fold and dimeric P2 species. The first hypothesis assumes that P2 oligomer constitutes the elementary unit of PrP^{Sc} assemblies and both constitute two phases in equilibrium (Figure8(B)). The balance between these two phases is then governed by the stacking energy of the elementary oligomeric unit and the law of mass action. An alternative hypothesis would be a spontaneous transformation of amyloid fibril assemblies into dimeric P2 species by a complex or assisted structural rearrangement at the monomeric protomer scale (Figure8(C)). In order to determine

which hypothesis is more likely, we can first consider the condensation hypothesis from a topological point of view.[43,44] Based on the high-resolution structure of PrP^{Sc} amyloid fibrils,[11–14] the equivalence of stacking interactions for each protomer in PIRIBS with its i-1 and i+1 neighbors highlights a monomeric protomer and discards the existence of a periodic oligomeric subunit. This argues against the fact that fibrils may result from a simple condensation of P2 species. Similar rationale can be done with all models where the elementary subunit is a monomer as is the case with the β-solenoid model.[45,46] The decondensation and transformation hypothesis can be also considered from an energetical point of view. The potential energy estimation of the asymmetric unit of RML fibrils at 2.70 Å resolution[14] (see materials and methods) is approximatively −14,000 kcal/mol. For comparison, the standard free energy of sheep recombinant PrP is approximately −9 kcal/mol,[47] and a carbon–carbon covalent bond and a disulfide bridge are approximately −60 kcal/mol and −58 kcal/mol, respectively.[48] It clearly appears that in comparison to the unfolding energy of recombinant PrP or to a covalent C–C and S-S bond, the stability of the RML PrP^{res} monofilament is high enough to render these assemblies unresponsive to a simple equilibrium displacement by dilution or change in ionic strength at 37 °C. Thus, structurally and energetically, a certain degree of structural transition should occur at the protomer level during the passage from a monomeric protomer in PIRIBS fold to P2 oligomers or vice versa. As the P2 species harbors the infectivity and all the attributes of the strain, this transformation is likely to predominantly affect the domain involved in the organization of the quaternary structure rather than the SSD. The even-more-complex to-tackle transformation hypothesis may explain why highly purified 263 K amyloid filaments spontaneously generated P2 without any P1, as reported in Figure 3.

Conclusion

The high dynamicity of PrP^{Sc} assemblies highlighted in the present work contrasts with the deadpan dogma of PrP^{Sc} assemblies. We highlighted that fibrillar architectures are not the unique quaternary structure organization harboring prion infective determinants, but alternative PrP^{Sc} assemblies such as small oligomeric species such as P1 and P2 also harbor infectivity and SSD. This duality led us to propose a folding-domain separation between the strain determinant and folding domain involved in the formation of the quaternary structure. The existence of such an alternative infectious quaternary structure also questions the principle of templating and fibril end-elongation as a unique mode of prion replication.

Materials and Methods

Ethics

Animal experiments were conducted in strict accordance with ECC and EU directives 86/009 and 2010/63 and were approved by the local ethics committee of the author's institution (Comethea; permit numbers 12/034, 15/045 and APAFIS#29603-2021020914525215).

Brain homogenate and purified 263 K preparation and solubilization

Stocks of infected brain homogenate (BH, 20% w/v in 5% glucose) from golden Syrian hamsters for the 263 K strain, from tg338 transgenic mice for the LA21K *fast* and LA19K strains, and from tga20 transgenic mice for the 22L, Fukuoka-1, ME7 and 139A strains were treated with 80 μg/mL PK for 1.5 h at 37 °C under gentle agitation. The reaction was stopped by the addition of Pefabloc at a final concentration of 2 mM in the BH. Prior to size exclusion chromatography (SEC), 200 μl BH was mixed with an equal volume of 200 μl solubilization buffer (2X concentrated) to reach a final concentration of 25 mM HEPES (stock 0.5 M, pH 7.4), 150 mM NaCl, 10 mM EDTA, 5 mM n-dodecyl β -D-maltoside (DM) and 50 mM sarkosyl. The mixture was then incubated at 37 °C for 4 h under gentle orbital agitation (300 rpm on Eppendorf Thermomixer) and centrifuged at 15,000*g* for 5 min prior to SEC analysis. Urea unfolding experiments were performed by providing 200 μl of BH followed by the addition of urea (solid) to the solubilization buffer to reach 1 to 7 M final urea concentration in the BH after the addition of solubilization buffer to the BH. As the addition of urea, specifically at high concentrations, causes a change in the sample volume, the amount of added water was adjusted to always ensure a constant concentration of the components of the solubilization in the final sample. 263 K PrP^{res} was purified and PK-treated according to the protocol described by Wenborn and colleagues.[34] Prior to SEC analysis, 500 ng of purified, PK-treated 263 K PrP^{res} was recovered in the solubilization buffer (as for brain homogenate) and incubated in the same condition as for the seven strains.

Size exclusion chromatography and quaternary structure determination

SEC analysis was performed using an ÄKTA-100 purifier FPLC (series 900, Amersham Biosciences, Amersham, UK) and a Superdex 200 10/300 GL gel filtration column (24 ml, GE, Chicago, US). The void volume and the total volume of the S200 column used here are 20 ml and 9.8 ml, respectively. In all SEC experiments, the sample loaded volume was 350 μl. The composition of the running buffer

was 25 mM HEPES and 150 mM NaCl, and the pH of the buffer was adjusted to pH 7.2. For ionic strength and urea experiments, the NaCl and urea concentrations of the running buffer and solubilized BH were identical. In all SEC experiments, no detergents were added to the running buffer to avoid the formation and maintenance of micellar structures.[32,33] After centrifugation at 10,000*g* for 3 min (no visible pellet), the entire sample solution was loaded on an SEC column using a sample loop. During elution, fractions of 250 μl were collected at 0.35 ml/min. Between each SEC run, the column was sanitized with three times the column volume of a 2 M sodium hydroxide. The column was calibrated using blue dextran molecules with varying molecular weights between 10 and 300 kDa, standard globular proteins (Bio-Rad), PrP^{C} and recPrP. The mean average molecular weight (<Mw>) as well as size distribution prior to any treatment of purified, PK-digested 263 K[34] assemblies was estimated by a homemade static light scattering (SLS) device and by dynamic light scattering (DLS, Malvern). The <Mw> of fractions obtained from SEC analysis of purified 263 K was determined according to the Rayleigh relation by normalizing the SLS intensity by the ratio of PrP.[49,50] Crosslinking was performed by incubating SEC fractions corresponding to the P1 and P2 peaks with the 11 Å bifunctional amine crosslinker bis-sulfosuccinimidyl suberate (BS3) at final concentrations of 0.5 mM and 2 mM for 15 min at 37 °C. The reaction was stopped by the addition of 1 mM Tris-buffer and analyzed by conventional western blot using Sha31b antibody.

Dilution experiments

For each prion strain, BH (20% w/v in 5% glucose) was first treated with 80 μg/ml PK for 1.5 h at 37 °C under gentle agitation. The reaction was stopped by the addition of Pefabloc to a final concentration of 2 mM. Then, the PK-treated BH was diluted by a given factor (1/2, 1/3, 1/5 and 1/10) in 5% glucose solution v/v prior to adding 2X solubilization buffer and incubation at 37 °C for 4 h under gentle orbital agitation (500 rpm on Eppendorf Thermomixer). The product was then analyzed by SEC as described earlier.

PrP quantification by western blot

Western blotting was used to quantify the amount of PrP in SEC fractions. SEC fractions were mixed with 4X Laemmli buffer (containing 6 M urea) and heated at 98 °C for 10 min. Samples were loaded onto 26-well 12% Bis-Tris Criterion XT precasted gels (Bio-Rad Laboratories Inc., Hercules, CA, USA) and electrotransferred onto nitrocellulose membranes with a semidry electrotransfer system (Schleicher & Schuell BioScience, Whatman). Immunoactivity was probed with biotinylated Sha31 antibody at 1/100,000 dilution[51] for 15–20 min at room temperature. Biotinylated Sha31 is revealed using HRP streptavidin (Sigma-Aldrich). For all SDS-PAGE analyses, a fixed quantity of human PrP was employed for consistent calibration of the PrP signals in different gels. To improve the sensitivity of the western detection method for samples containing low levels of PrP^{res}, double deposition was performed to electroconcentrate the sample, as previously described.[30] Typically, after a first round of sample loading in SDS-PAGE wells, a short, 2 min migration at 160 V was performed to allow sample migration within the acrylamide gel for less than 2 mm. This was followed by a second round of sample loading before the migration was continued at 160 V for 20 min until the front reached 3 cm within the gel. Longer time or higher voltage for the entrance of the first load led to the formation of doublet in the blots. Electrotransfer and detection remained unchanged.

Miniaturized bead-PMCA assay

Protein misfolding cyclic amplification was conducted according to a method first developed by Soto et al.[52] and further optimized in-house by Moudjou et al.[53] Briefly, serial ten-fold dilutions of SEC fractions from LA21K *fast* and 263 K prions (diluted in PMCA buffer) were mixed with brain lysates (10% wt/vol) from healthy tg338 and tg7 mice as respective substrates and subjected to one round of 96 cycles of 30-s sonications (220–240 Watts) followed by 29.5 min of incubation at 37 °C. PMCA was performed in a 96-well microplate format (Axygen, Corning) using a Q700 sonicator (QSonica, USA, Delta Labo, Colombelles, France). The amplified products were PK-digested (115 μg/ml final concentration, 0.6% SDS, 1 h, 37 °C) prior to immunoblot analyses, as described above.

Bioassays

Bioassays were performed on pools of fractions corresponding to elution volumes between 13.23 ml to 13.98 ml for P1, 15.48 ml to 16.26 ml for P2, 13.46 ml to 13.95 ml for $P1^{U}$ and 8.98 ml to 9.97 ml for $P0^{U}$ (see SI3). Practically, the pool of fractions of interest was extemporarily diluted fivefold in 5% glucose and immediately inoculated via the intracerebral route into reporter mice tg338 and tg7 (20 μl per pool of fractions, $n = 5$ mice per pool). Mice showing prion-specific neurological symptoms were euthanized at the end stage. To confirm the presence of prion disease, brains were removed and analyzed for PrP^{Sc} content using the Bio-Rad TsSeE detection kit prior to immunoblotting, as described above. The survival time was defined as the number of days from inoculation to euthanasia. To estimate the mean relative infectious dose of each fraction, previously established, strain-specific curves correlating the

relative infectious dose to survival times were used.[19,35] As input reference, animals inoculated with 2 mg of infectious brain tissue are assigned a relative dose of 0. Specific infectivity values were then calculated by dividing the relative infectious dose by the amount of PrP^{res} present in each inoculated peak. This amount was estimated based on the percentage of PrP^{res} reported on chromatograms (see SI3).

Energy calculation

The potential energy of the asymmetric unit of RML PrP assemblies (PDB:7quig,[14]) was estimated using the Amber 20 suite of programs. Hydrogens were added to the structures and the energies were minimized (max cycle = 1000) in the implicit solvent model (igb = 8, cutoff = 1000 Å) with the ff14SBonlysc force field to eliminate clashes without altering the original structure. In order to not modify the overall structure, the potential energy was calculated at 0°K.

Author Contributions

A.I., V.B. and H.R. designed the research; all authors contributed to the research and analyzed the data; and V.B., J.B., A.I. and H.R. wrote the paper.

CRediT authorship contribution statement

Jan Bohl: Investigation, Validation, Conceptualization, Writing – original draft. **Mohammed Moudjou:** Investigation, Formal analysis. **Laetitia Herzog:** Investigation. **Fabienne Reine:** Investigation. **Fiona Sailer:** Investigation. **Hannah Klute:** Investigation. **Frederic Halgand:** Investigation. **Guillaume Van der Rest:** Investigation. **Yves Boulard:** Software, Methodology, Formal analysis. **Vincent Béringue:** Project administration, Supervision, Validation, Investigation, Writing – review & editing. **Angelique Igel:** Project administration, Conceptualization, Supervision, Validation, Investigation, Writing – review & editing, Writing – original draft. **Human Rezaei:** Project administration, Supervision, Validation, Investigation, Writing – review & editing.

DATA AVAILABILITY

Data will be made available on request.

DECLARATION OF COMPETING INTEREST

The authors declare that they have no known competing financial interests or personal relationships that could have appeared to influence the work reported in this paper.

Acknowledgments

This work was supported by grants from the Fondation pour la Recherche Médicale (Equipe FRM DEQ20150331689), the European Research Council (ERC Starting Grant SKIPPERAD, number 306321), the Ile de France region (DIM MALINF), Metaprogramme Digit-Bio (PrionDiff) and the support of Hochschule Fresenius university.

Appendix A. Supplementary data

Supplementary data to this article can be found online at https://doi.org/10.1016/j.jmb.2023.168280.

Received 21 March 2023;
Accepted 11 September 2023;
Available online 18 September 2023

Keywords:
prion;
dynamicity;
strains;
oligomer;
heterogeneity

References

1. Come, J.H., Fraser, P.E., Lansbury Jr., P.T., (1993). A kinetic model for amyloid formation in the prion diseases: importance of seeding. *PNAS* **90**, 5959–5963.
2. Telling, G.C., Parchi, P., DeArmond, S.J., Cortelli, P., Montagna, P., Gabizon, R., et al., (1996). Evidence for the conformation of the pathologic isoform of the prion protein enciphering and propagating prion diversity. *Science* **274**, 2079–2082.
3. McKinley, M.P., Braunfeld, M.B., Bellinger, C.G., Prusiner, S.B., (1986). Molecular characteristics of prion rods purified from scrapie-infected hamster brains. *J Infect Dis* **154**, 110–120.
4. Kocisko, D.A., Come, J.H., Priola, S.A., Chesebro, B., Raymond, G.J., Lansbury, P.T., et al., (1994). Cell-free formation of protease-resistant prion protein. *Nature* **370**, 471–474.
5. Bessen, R.A., Kocisko, D.A., Raymond, G.J., Nandan, S., Lansbury, P.T., Caughey, B., (1995). Non-genetic propagation of strain-specific properties of scrapie prion protein. *Nature* **375**, 698–700.
6. Chien, P., Weissman, J.S., DePace, A.H., (2004). Emerging principles of conformation-based prion inheritance. *Annu. Rev. Biochem* **73**, 617–656.
7. Griffith, J.S., (1967). Self-replication and scrapie. *Nature* **215**, 1043–1044.

8. Lansbury Jr., P.T., Caughey, B., (1995). The chemistry of scrapie infection: implications of the 'ice 9' metaphor. *Chem. Biol.* **2**, 1–5.
9. Bruce, M.E., (2003). TSE strain variation. *Br. Med. Bull.* **66**, 99–108.
10. Beringue, V., Vilotte, J.L., Laude, H., (2008). Prion agent diversity and species barrier. *Vet. Res.* **39**, 47.
11. Hoyt, F., Alam, P., Artikis, E., Schwartz, C.L., Hughson, A. G., Race, B., et al., (2022). Cryo-EM of prion strains from the same genotype of host identifies conformational determinants. *PLoS Pathog.* **18**, e1010947.
12. Hoyt, F., Standke, H.G., Artikis, E., Schwartz, C.L., Hansen, B., Li, K., et al., (2022). Cryo-EM structure of anchorless RML prion reveals variations in shared motifs between distinct strains. *Nature Commun.* **13**, 4005.
13. Kraus, A., Hoyt, F., Schwartz, C.L., Hansen, B., Artikis, E., Hughson, A.G., et al., (2021). High-resolution structure and strain comparison of infectious mammalian prions. *Mol. Cell* **81** (4540–51), e6.
14. Manka, S.W., Zhang, W., Wenborn, A., Betts, J., Joiner, S., Saibil, H.R., et al., (2022). 2.7 A cryo-EM structure of ex vivo RML prion fibrils. *Nature Commun.* **13**, 4004.
15. Manka, S.W., Wenborn, A., Betts, J., Joiner, S., Saibil, H. R., Collinge, J., et al., (2023). A structural basis for prion strain diversity. *Nature Chem. Biol.*.
16. Bessen, R.A., Marsh, R.F., (1994). Distinct PrP properties suggest the molecular basis of strain variation in transmissible mink encephalopathy. *J. Virol.* **68**, 7859–7868.
17. Peretz, D., Williamson, R.A., Legname, G., Matsunaga, Y., Vergara, J., Burton, D.R., et al., (2002). A change in the conformation of prions accompanies the emergence of a new prion strain. *Neuron* **34**, 921–932.
18. Legname, G., Nguyen, H.O., Peretz, D., Cohen, F.E., DeArmond, S.J., Prusiner, S.B., (2006). Continuum of prion protein structures enciphers a multitude of prion isolate-specified phenotypes. *PNAS* **103**, 19105–19110.
19. Tixador, P., Herzog, L., Reine, F., Jaumain, E., Chapuis, J., Le Dur, A., et al., (2010). The physical relationship between infectivity and prion protein aggregates is strain-dependent. *PLoS Pathog.* **6**, e1000859.
20. Safar, J.G., Xiao, X., Kabir, M.E., Chen, S., Kim, C., Haldiman, T., et al., (2015). Structural determinants of phenotypic diversity and replication rate of human prions. *PLoS Pathog.* **11**, e1004832.
21. Laferriere, F., Tixador, P., Moudjou, M., Chapuis, J., Sibille, P., Herzog, L., et al., (2013). Quaternary structure of pathological prion protein as a determining factor of strain-specific prion replication dynamics. *PLoS Pathog.* **9**, e1003702.
22. Bishop, M.T., Will, R.G., Manson, J.C., (2010). Defining sporadic Creutzfeldt-Jakob disease strains and their transmission properties. *PNAS* **107**, 12005–12010.
23. Jaumain, E., Quadrio, I., Herzog, L., Reine, F., Rezaei, H., Andreoletti, O., et al., (2016). Absence of evidence for a causal link between bovine spongiform encephalopathy strain variant L-BSE and known forms of sporadic Creutzfeldt-Jakob disease in human PrP transgenic mice. *J. Virol.* **90**, 10867–10874.
24. Le Dur, A., Lai, T.L., Stinnakre, M.G., Laisne, A., Chenais, N., Rakotobe, S., et al., (2017). Divergent prion strain evolution driven by PrP(C) expression level in transgenic mice. *Nature Commun.* **8**, 14170.
25. Nakic, N., Tran, T.H., Novokmet, M., Andreoletti, O., Lauc, G., Legname, G., (2021). Site-specific analysis of N-glycans from different sheep prion strains. *PLoS Pathog.* **17**, e1009232.
26. Artikis, E., Kraus, A., Caughey, B., (2022). Structural biology of ex vivo mammalian prions. *J. Biol. Chem.* **298**, 102181
27. Li, J., Browning, S., Mahal, S.P., Oelschlegel, A.M., Weissmann, C., (2010). Darwinian evolution of prions in cell culture. *Science* **327**, 869–872.
28. Collinge, J., Clarke, A.R., (2007). A general model of prion strains and their pathogenicity. *Science* **318**, 930–936.
29. Igel, A., Fornara, B., Rezaei, H., Beringue, V., (2022). Prion assemblies: structural heterogeneity, mechanisms of formation, and role in species barrier. *Cell Tissue Res.*.
30. Igel-Egalon, A., Laferriere, F., Moudjou, M., Bohl, J., Mezache, M., Knapple, T., et al., (2019). Early stage prion assembly involves two subpopulations with different quaternary structures and a secondary templating pathway. *Commun Biol.* **2**, 363.
31. Wittig, I., Schagger, H., (2009). Native electrophoretic techniques to identify protein-protein interactions. *Proteomics* **9**, 5214–5223.
32. Tao, H., Liu, W., Simmons, B.N., Harris, H.K., Cox, T.C., Massiah, M.A., (2010). Purifying natively folded proteins from inclusion bodies using sarkosyl, Triton X-100, and CHAPS. *Biotechniques* **48**, 61–64.
33. Medina, R., Perdomo, D., Bubis, J., (2004). The hydrodynamic properties of dark- and light-activated states of n-dodecyl beta-D-maltoside-solubilized bovine rhodopsin support the dimeric structure of both conformations. *J. Biol. Chem.* **279**, 39565–39573.
34. Wenborn, A., Terry, C., Gros, N., Joiner, S., D'Castro, L., Panico, S., et al., (2015). A novel and rapid method for obtaining high titre intact prion strains from mammalian brain. *Sci. Rep.* **5**, 10062.
35. Igel-Egalon, A., Laferriere, F., Tixador, P., Moudjou, M., Herzog, L., Reine, F., et al., (2020). Crossing species barriers relies on structurally distinct prion assemblies and their complementation. *Mol. Neurobiol.* **57**, 2572–2587.
36. Langevin, C., Andreoletti, O., Le Dur, A., Laude, H., Beringue, V., (2011). Marked influence of the route of infection on prion strain apparent phenotype in a scrapie transgenic mouse model. *Neurobiol. Dis.* **41**, 219–225.
37. Moudjou, M., Sibille, P., Fichet, G., Reine, F., Chapuis, J., Herzog, L., et al., (2013). Highly infectious prions generated by a single round of microplate-based protein misfolding cyclic amplification. *MBio* **5**, e00829–e00913.
38. Ellett, L.J., Revill, Z.T., Koo, Y.Q., Lawson, V.A., (2020). Strain variation in treatment and prevention of human prion diseases. *Prog. Mol. Biol. Transl. Sci.* **175**, 121–145.
39. Boyle, A., Hogan, K., Manson, J.C., Diack, A.B., (2017). Strain typing of prion diseases using in vivo mouse models. *Methods Mol. Biol.* **1658**, 263–283.
40. Igel-Egalon, A., Moudjou, M., Martin, D., Busley, A., Knapple, T., Herzog, L., et al., (2017). Reversible unfolding of infectious prion assemblies reveals the existence of an oligomeric elementary brick. *PLoS Pathog.* **13**, e1006557.
41. Vanni, I., Pirisinu, L., Acevedo-Morantes, C., Kamali-Jamil, R., Rathod, V., Di Bari, M.A., et al., (2020). Isolation of infectious, non-fibrillar and oligomeric prions from a genetic prion disease. *Brain* **143**, 1512–1524.

42. Pastrana, M.A., Sajnani, G., Onisko, B., Castilla, J., Morales, R., Soto, C., et al., (2006). Isolation and characterization of a proteinase K-sensitive PrPSc fraction. *Biochemistry* **45**, 15710–15717.
43. Grazioli, G., Yu, Y., Unhelkar, M.H., Martin, R.W., Butts, C. T., (2019). Network-based classification and modeling of amyloid fibrils. *J. Phys. Chem. B* **123**, 5452–5462.
44. Ahnert, S.E., Marsh, J.A., Hernandez, H., Robinson, C.V., Teichmann, S.A., (2015). Principles of assembly reveal a periodic table of protein complexes. *Science* **350**, aaa2245.
45. Vazquez-Fernandez, E., Vos, M.R., Afanasyev, P., Cebey, L., Sevillano, A.M., Vidal, E., et al., (2016). The structural architecture of an infectious mammalian prion using electron cryomicroscopy. *PLoS Pathog.* **12**, e1005835.
46. Spagnolli, G., Rigoli, M., Orioli, S., Sevillano, A.M., Faccioli, P., Wille, H., et al., (2019). Full atomistic model of prion structure and conversion. *PLoS Pathog.* **15**, e1007864.
47. Rezaei, H., Choiset, Y., Eghiaian, F., Treguer, E., Mentre, P., Debey, P., et al., (2002). Amyloidogenic unfolding intermediates differentiate sheep prion protein variants. *J. Mol. Biol.* **322**, 799–814.
48. Sheu, S.Y., Yang, D.Y., Selzle, H.L., Schlag, E.W., (2003). Energetics of hydrogen bonds in peptides. *PNAS* **100**, 12683–12687.
49. Lorber, B., Fischer, F., Bailly, M., Roy, H., Kern, D., (2012). Protein analysis by dynamic light scattering: methods and techniques for students. *Biochem. Mol. Biol. Educ.* **40**, 372–382.
50. Sahin, E., Roberts, C.J., (2012). Size-exclusion chromatography with multi-angle light scattering for elucidating protein aggregation mechanisms. *Methods Mol. Biol.* **899**, 403–423.
51. Feraudet, C., Morel, N., Simon, S., Volland, H., Frobert, Y., Creminon, C., et al., (2005). Screening of 145 anti-PrP monoclonal antibodies for their capacity to inhibit PrPSc replication in infected cells. *J. Biol. Chem.* **280**, 11247–11258.
52. Saborio, G.P., Permanne, B., Soto, C., (2001). Sensitive detection of pathological prion protein by cyclic amplification of protein misfolding. *Nature* **411**, 810–813.
53. Moudjou, M., Chapuis, J., Mekrouti, M., Reine, F., Herzog, L., Sibille, P., et al., (2016). Glycoform-independent prion conversion by highly efficient, cell-based, protein misfolding cyclic amplification. *Sci. Rep.* **6**, 29116.
54. Loster, K., Josic, D., (1997). Analysis of protein aggregates by combination of cross-linking reactions and chromatographic separations. *J. Chromatogr. B Biomed. Sci. Appl.* **699**, 439–461.